Journal of Computational Science 101 (2026) 102996

Contents lists available at ScienceDirect

Journal of Computational Science

journal homepage: www.elsevier.com/locate/jocs

Expedited microwave optimization using variable-fidelity EM analysis and convergence/quality-driven model adjustment

Slawomir Koziel [a,b,*], Anna Pietrenko-Dabrowska [b]

[a] Engineering Optimization & Modeling Center, Reykjavik University, Reykjavik 101, Iceland
[b] Faculty of Electronics, Telecommunications and Informatics, Gdansk University of Technology, Gdansk 80-233, Poland

ARTICLE INFO

Keywords:
Microwave circuits
EM-based design
Variable-fidelity simulations
Model adjustment
Parameter tuning
Gradient methods

ABSTRACT

Electromagnetic (EM)-based optimization is imperative for most microwave circuits. This is because designs produced by circuit theory methods require further adjustments to ensure satisfactory performance. Unfortunately, repetitive EM simulations incurred by optimization procedures are associated with considerable expenses. Expediting the process is essential to reduce the time span of design cycles and time-to-market in the case of industrial products. One possibility is utilization of variable-resolution EM simulations; however, available frameworks typically employ two discrete levels of fidelity (coarse/fine) combined with often sophisticated model correction methods. This paper proposes an alternative approach to accelerated microwave component tuning. Our methodology involves a continuous spectrum of EM simulation resolutions, which are controlled using the convergence and design quality indicators of the underlying optimization routine. A management scheme adjusting the model resolution is developed to utilize the lowest usable resolution at the search process onset, which is continuously increased as the algorithm approaches convergence and the objective function reaches satisfactory levels. The final stages are carried out with high-fidelity resolution to ensure accuracy. Verification experiments conducted using three microstrip circuits demonstrate over sixty percent of average savings over the reference (single-resolution) gradient-based routine, and noticeable and consistent acceleration regarding several state-of-the-art expedited versions. Selected designs are experimentally validated.

1. Introduction

Electromagnetic (EM) simulation has become fundamental in microwave design [1–4]. The primary reason is the ability of EM simulation to quantify mutual coupling, the impact of the circuit environment (connectors, housing), substrate anisotropy, or multi-physics phenomena [5–8], which cannot be quantified otherwise. Evaluation reliability is essential for complex circuits developed to meet the needs of emerging applications (5 G, energy harvesting, space communications, wireless power transfer [9–12]), compact systems [13–15], and those realizing functionalities that enable hardware re-use (dual-, multi-band capability [16–19], reconfigurability [20], custom phase responses [21]). The challenge pertinent to the development of geometrically sophisticated circuits is the need for meticulous adjustment of multiple parameters, which entails repetitive EM analyses. The accumulated cost thereof might be impractically high even for local tuning [22–24], let alone global optimization (frequently realized by means of bio-inspired methods [25–28]), or uncertainty quantification [29,30].

Expediting EM-based procedures has been extensively researched. Some of existing methodologies are gradient-based routines expedited through adjoint sensitivities or other methods reducing the computational burden related to sensitivity evaluation (mesh deformation, sparse Jacobian updating schemes) [31–36]. In recent years, an increasing interest in surrogate-assisted methods was observed regarding data-driven and physics-enabled ones [37–40]. Behavioral modelling is more popular due to accessibility of third-party toolboxes [41,42], and includes a broad range of techniques (kriging, support vector regression, neural networks, polynomial chaos expansion [43–47]). Yet, modelling microwave circuit responses over broad parameter ranges and frequencies is extremely difficult. Consequently, practical surrogate-based frameworks are typically implemented as machine learning (ML) procedures. Therein, the metamodel is iteratively enhanced and applied as a low-cost predictor [48–52]. Due to the mentioned challenges, suitability of ML methods is restricted to relatively simple devices [53,54]. Physics-enabled offer improved immunity to dimensionality-related challenges while being less versatile as the

* Corresponding author at: Engineering Optimization & Modeling Center, Reykjavik University, Reykjavik 101, Iceland.
E-mail addresses: koziel@ru.is (S. Koziel), anna.dabrowska@pg.edu.pl (A. Pietrenko-Dabrowska).

https://doi.org/10.1016/j.jocs.2026.102996
Received 4 December 2025; Received in revised form 17 July 2026; Accepted 3 August 2026
Available online 12 August 2026
1877-7503/

Symbol	Explanation
$\boldsymbol{x} = [x_1 \ldots x_n]^T$	Vector of designable variables, typically geometry parameters of the microwave circuit
$U(\boldsymbol{x})$	Scalar objective function defined so that a better design corresponds to a lower value of U
$g_k(\boldsymbol{x}) \leq 0$, $k = 1, \ldots, n_g$	Optional inequality constraints
$h_k(\boldsymbol{x}) = 0$, $k = 1, \ldots, n_h$	Optional equality constraints
$S_{kl}(\boldsymbol{x},f)$	Scattering parameters: f stands for the frequency; k and l denote the circuit ports

(a)

Design optimization problem: identify optimum vector of design parameters $\boldsymbol{x}^*$ so that

$$\boldsymbol{x}^* = \arg\min_{\boldsymbol{x}} U(\boldsymbol{x}) \tag{1}$$

Constrained optimization problem with implicit constraint handling (cf. [74])

$$\boldsymbol{x}^* = \arg\min_{\boldsymbol{x}} U_P(\boldsymbol{x}) \tag{2}$$

where U_P is a compound of the function U and the penalty terms of the form

$$U_P(\boldsymbol{x}) = U(\boldsymbol{x}) + \sum_{k=1}^{n_g+n_h} \beta_k c_k(\boldsymbol{x}) \tag{3}$$

Remark 1: $c_k(\boldsymbol{x})$ quantify constraint violations, whereas β_k are the penalty coefficients.
Remark 2: Penalty function example: assume constraint $S(\boldsymbol{x}) = \max\{S_1(\boldsymbol{x}), S_4(\boldsymbol{x})\} \leq -20$ dB (S_1 and S_4 being the maximum in-band reflection and port isolation, respectively); we have $c(\boldsymbol{x}) = [(S(\boldsymbol{x}) + 20)/20]^2$. The second power ensures smoothness of U_P at boundary of the feasible region. The power factor also controls the stiffness of the constraint, with the second power enabling tolerance for small violations.

(b)

Fig. 1. EM-driven microwave optimization. Formulation of the problem: (a) terminology, (b) design task.

lower-fidelity models are problem-dependent [55–58]. Yet another group of methods are feature-based techniques [59,60], offering potentially tremendous computational benefits at the expense of being contingent upon the existence of so-called characteristics points of the circuit responses [60].

Given a plethora of available optimization methods, it should be emphasized that globalized search is used rather sparsely (e.g., design of metasurfaces, synthesis of antenna array patterns, frequency-selective surfaces [61–63], parameter adjustment of compact structures based on CMRCs [64]). Most EM-driven tasks are related to local tuning, most often realized using gradient-based search. The reason is that decent starting points are frequently generated at the early steps of circuit development. The acceleration methods applicable for gradient algorithms include the adjoint sensitivities mentioned. Notwithstanding, it is an intrusive methodology, and it is not readily available through commercial EM solvers. Sparse sensitivity updating schemes [65–67] are more straightforward to implement and offer up to fifty percent savings while presenting noticeable quality deterioration. On the other hand, variable-resolution algorithms may be remarkably efficient, but they are heavily reliant on appropriate arrangement (choosing the low-fidelity representation and its augmentation techniques) [56,68,69]. Increasing the number of model fidelities may be beneficial [70], yet a practical issue is model handling, e.g., selecting the proper resolution levels [71]. Recently, a model adjustment scheme was suggested [72], with the model resolution adjusted continuously utilizing convergence indicators. The method of [72] is rather intrinsic to implement and requires restarting the search process upon premature convergence (i.e., if the resolution level did not reach the maximum assumed level). On the other hand, it offers considerable computational advantages over the baseline (single resolution) procedure.

This paper proposes an alternative model management scheme with the EM analysis level chosen from a continuous family of resolutions, which might be adjusted between the lowest and the high-fidelity one. The resolution adjustment is guided by the convergence and design quality indicators. In particular, the lowest resolution is used early in the search process and continuously increases when the algorithm approaches convergence and the objective function value reach satisfactory levels. Making the model fidelity a function of system quality leads to additional speedup. This is achieved by limiting the waste of computational resources on poor designs. Extensive verification experiments demonstrate excellent performance of the presented technique with computational savings of up to 74 % with only minor reliability degradation. At the same time, the presented approach is competitive to several accelerated procedures. Another attractive feature of the discussed method is its simple implementation and handling.

2. Convergence-quality model management for expedited variable-resolution microwave optimization

In this part of the paper, we elaborate the proposed optimization procedure. The focus is on variable-resolution EM modelling and model fidelity handling. The design problem statement (Section 2.1) is followed by outlining a conventional gradient-based algorithm to be used as a baseline algorithm (Section 2.2), characterization of variable-resolution simulations (Section 2.3), and convergence/quality-dependent model management (Section 2.4). The complete algorithm is summarized in Section 2.5.

Design scenario: verbal description	Objective function
Circuit: Dual-band coupler Objectives: • Operating frequencies f_1 and f_2 • Ensure equal power split at both f_1 and f_2 • Minimization of the circuit matching and isolation responses at f_1 and f_2	$U_P(\boldsymbol{x}) = \max\{S_{11}(\boldsymbol{x},f_1), S_{11}(\boldsymbol{x},f_2), S_{41}(\boldsymbol{x},f_1), S_{41}(\boldsymbol{x},f_1)\}$ $+\beta\left[\lvert S_{21}(\boldsymbol{x},f_1)-S_{31}(\boldsymbol{x},f_1)\rvert^2 + \lvert S_{21}(\boldsymbol{x},f_2)-S_{31}(\boldsymbol{x},f_2)\rvert^2\right]$
Circuit: Compact rat-race coupler Objectives: • Minimize the footprint area $A(\boldsymbol{x})$ • Ensure equal power split at the target frequency f_0 • Maintain $\lvert S_{11}\rvert$, $\lvert S_{41}\rvert \le -20$ dB over the bandwidth $[f_0 - B, f_0 + B]$	$U_P(\boldsymbol{x}) = A(\boldsymbol{x}) + \beta_1\left[\max\{c(\boldsymbol{x})+20, 0\}/20\right]^2 +$ $+\beta_2\left[\lvert S_{21}(\boldsymbol{x},f_0)\rvert - \lvert S_{31}(\boldsymbol{x},f_0)\rvert\right]^2$ where $c(\boldsymbol{x}) = \max\left\{\begin{matrix} f\in[f_0-B, f_0+B]: \\ \max\{\lvert S_{11}(\boldsymbol{x},f)\rvert, \lvert S_{41}(\boldsymbol{x},f)\rvert\}\end{matrix}\right\}$
Circuit: Triple-band power divider Objectives: • Operating frequencies f_1, f_2, and f_3 • Ensure equal power split at f_1, f_2, and f_3 • Minimize the circuit input matching $\lvert S_{11}\rvert$, output matching $\lvert S_{22}\rvert$ and $\lvert S_{33}\rvert$ at f_1, f_2, and f_3 • Minimize isolation $\lvert S_{23}\rvert$ at f_1, f_2, and f_3	$U_P(\boldsymbol{x}) = \max\left\{\max_{k,l\in\{1,2,3\}} S_{kk}(\boldsymbol{x},f_l), \max_{l\in\{1,2,3\}} S_{23}(\boldsymbol{x},f_l)\right\}$ $+\beta\sum_{l=1}^{3}\lvert S_{21}(\boldsymbol{x},f_l)-S_{31}(\boldsymbol{x},f_l)\rvert^2$

Fig. 2. EM-driven microwave optimization. Examples of representative design optimization scenarios.

Problem statement: Solve $\boldsymbol{x}^* = \text{argmin}\{\boldsymbol{x} \in X : U_P(\boldsymbol{x})\}$ (cf. (2))

Algorithm operation: Generate a series $\boldsymbol{x}^{(i)}$, i = 0, 1, …, of approximations to $\boldsymbol{x}^*$, with $\boldsymbol{x}^{(0)}$ being an initial design. The new vector $\boldsymbol{x}^{(i+1)}$ is obtained by solving

$$\boldsymbol{x}^{(i+1)} = \arg\min_{\boldsymbol{x};\,\|\boldsymbol{x}-\boldsymbol{x}^{(i)}\|\le d^{(i)}} U_L^{(i)}(\boldsymbol{x}) \tag{4}$$

where $U_L^{(i)}$ is analytically identical to U but evaluated using the first-order approximation model $\boldsymbol{L}^{(i)}(\boldsymbol{x})$ of the EM-simulated circuit responses $\boldsymbol{R}(\boldsymbol{x})$, defined at $\boldsymbol{x}^{(i)}$ as

$$\boldsymbol{L}^{(i)}(\boldsymbol{x}) = \boldsymbol{R}(\boldsymbol{x}^{(i)}) + \boldsymbol{J}_R(\boldsymbol{x}^{(i)})\cdot(\boldsymbol{x}-\boldsymbol{x}^{(i)}) \tag{5}$$

The Jacobian matrix $\boldsymbol{J}_R$ is estimated using finite differentiation.

Gain ratio r: EM-evaluated versus linear-model predicted objective function improvement

$$r = \frac{U_P(\boldsymbol{x}^{(i+1)},F) - U_P(\boldsymbol{x}^{(i)},F)}{U_L(\boldsymbol{x}^{(i+1)},\boldsymbol{L}^{(i)}(\boldsymbol{x}^{(i+1)}),F) - U_L(\boldsymbol{x}^{(i)},\boldsymbol{L}^{(i)}(\boldsymbol{x}^{(i)}),F)} \tag{6}$$

Trust region size $d^{(i)} > 0$: Adaptively adjusted based on r, $d^{(i+1)} = d^{(i)}m_{incr}$ if $r > r_{incr}$, and $d^{(i+1)} = d^{(i)}/m_{decr}$ if $r < r_{decr}$; standard control parameter values are $r_{incr} = 0.75$, $r_{decr} = 0.25$, $m_{incr} = 1.5$, $m_{decr} = 2$ [75].

Acceptance of the new iteration point: $\boldsymbol{x}^{(i+1)}$ is accepted only if $r > 0$ (i.e., EM-evaluated objective function has been improved); otherwise, the iteration is repeated with reduced TR size;

Algorithm termination: Convergence in argument ($\|\boldsymbol{x}^{(i+1)} - \boldsymbol{x}^{(i)}\| < \varepsilon_{TR}$) or sufficient reduction of the TR size ($d^{(i)} \le \varepsilon_{TR}$); the termination threshold is set to $\varepsilon_{TR} = 10^{-3}$

Fig. 3. Operating principles of the baseline TR algorithm.

2.1. Microwave circuit optimization. Problem formulation

As elaborated on in Section 1, initial designs obtained using circuit theory methods [73] must be further tuned to achieve satisfactory operation and boost the performance. The essential components of this process include a selection of adjustable parameters and defining the merit function (quantifying the design quality), and optional constraints. If multiple design goals are present, they are typically handled by selecting the main goal and casting other objectives into constraints. Proper multi-objective optimization (e.g., [27,52]) is not within the scope of this study. Fig. 1 gathers the notation used in the context of design optimization and analytical problem formulation. Fig. 2 collects representative design endeavors and the associated merit functions.

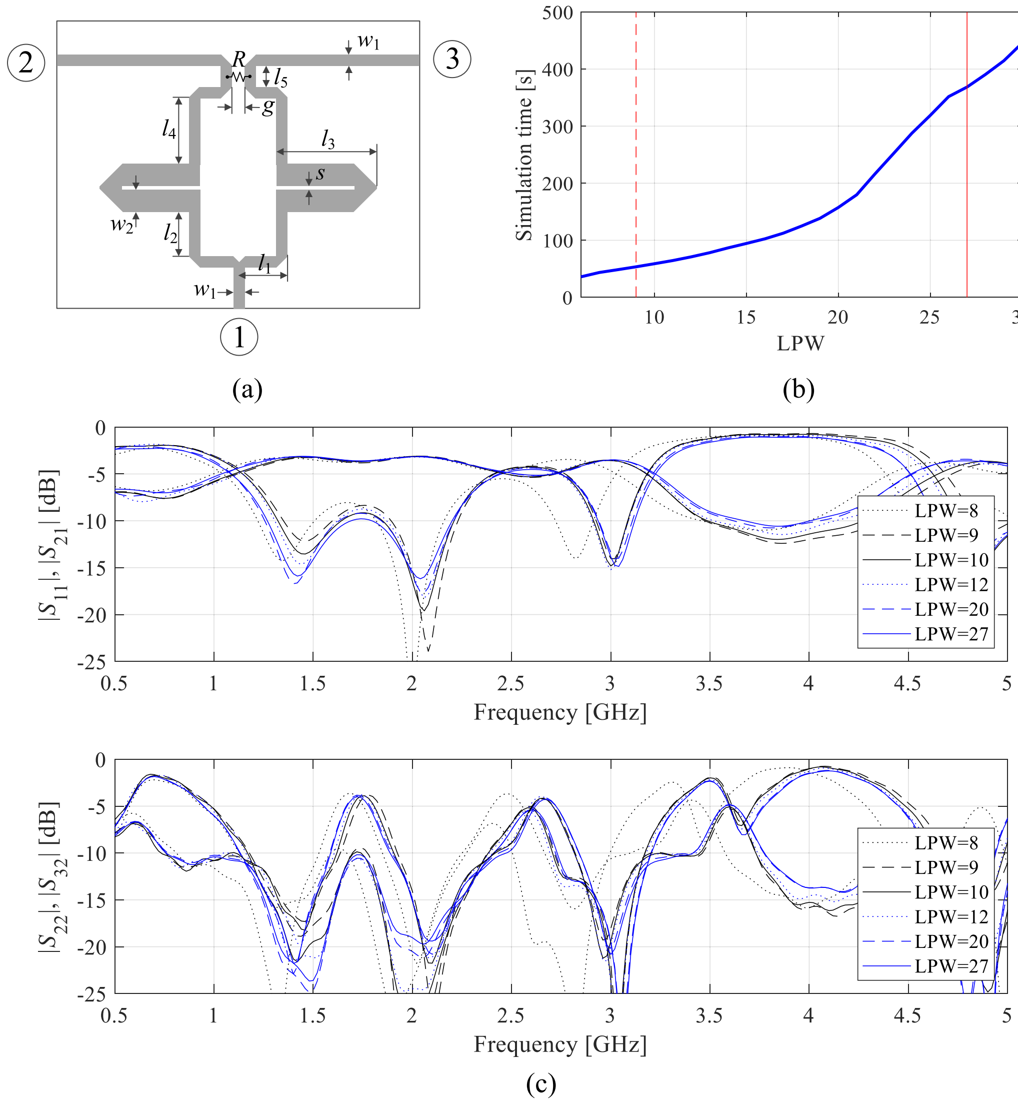

Fig. 4. Multi-fidelity EM-analysis for a power divider: (a) circuit architecture, (b) evaluation time vs. mesh density (controlled by LPW), (c) S-parameter responses for selected LPWs. The mesh density of the high-fidelity model (—), and the lowest low-fidelity one (- - -), are represented by vertical lines.

Symbol	Meaning	Default value
$Q_{c.\min}$	Lower bound on Q_c to determine whether optimization is near convergence ($Q_c^{(i)} < Q_{c.\min}$)	1 (one decade from convergence on a logarithmic scale)
$Q_{c.\max}$	Upper bound on Q_c to determine whether the process is away from convergence ($Q_c^{(i)} > Q_{c.\max}$)	3
$Q_{q.\min}$	Lower bound on Q_q to determine whether the design quality is satisfactory ($Q_q^{(i)} < Q_{q.\min}$)	Problem dependent, e.g., 0 dB for a constrained objective function defined to minimize in-band reflection/isolation
$Q_{q.\max}$	Upper bound on Q_q to determine whether the design quality is poor ($Q_q^{(i)} > Q_{q.\max}$)	Problem dependent, e.g., –15 dB for a constrained objective function defined to minimize in-band reflection/isolation

Fig. 5. Control parameters used by the proposed variable-resolution model management scheme.

2.2. Baseline algorithm: trust-region optimization with finite-difference gradients

The variable-resolution approach and the associated model management introduced in this paper can be combined—in principle—with any iterative optimization procedure.

The optimization algorithm considered here is the trust-region (TR) procedure [74] with the system response Jacobian calculated through finite differences. It is perhaps the most representative local tuning method utilized in high-frequency engineering. A variation of this

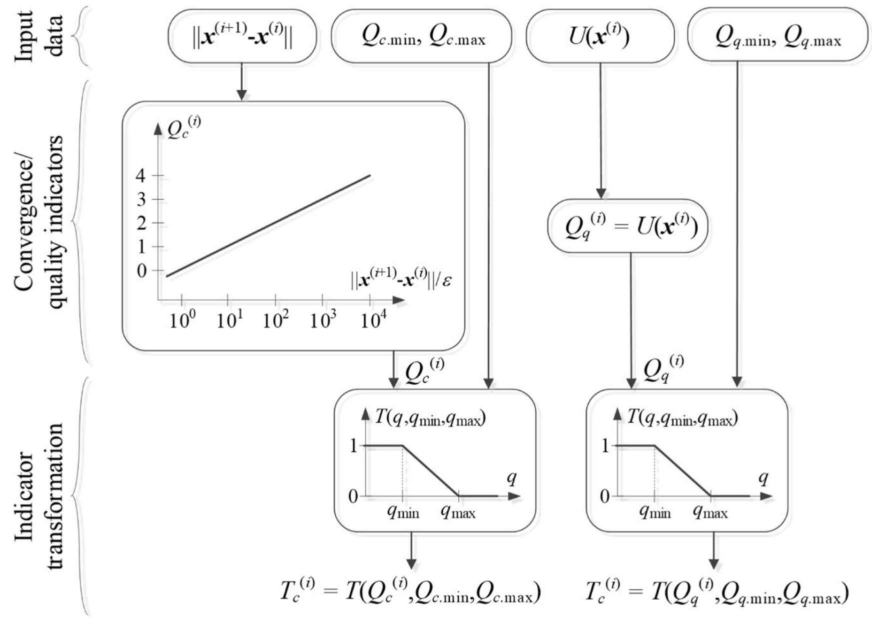

Fig. 6. Convergence and quality indicator computation (8), (9), and their transformation using the transition function T of (10).

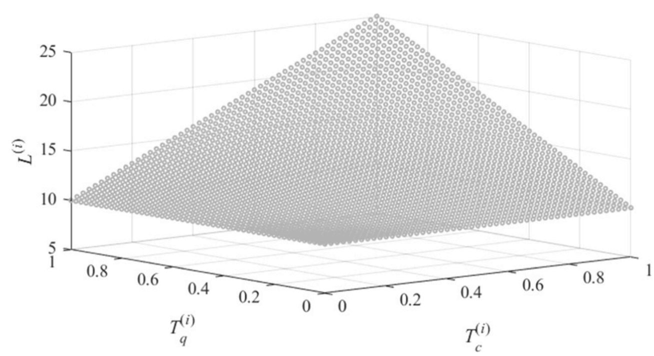

Fig. 7. Model fidelity $L^{(i)}$ as a function of transformed convergence and quality indicators, here, assuming $L_{min} = 10$, and $L_{max} = 25$.

procedure is available in CST Microwave Studio [75]. The main TR algorithm steps are outlined in Fig. 3. The candidate designs $\boldsymbol{x}^{(i+1)}$ rendered in the ith iteration are found by optimizing the first-order linear model $\boldsymbol{L}^{(i)}$, which acts as a predictor replacing EM-simulated collected circuit outputs marked as $\boldsymbol{R}(\boldsymbol{x})$. The search region size $d^{(i)}$ is controlled using the prediction quality quantified using the gain ratio r. The specific form of $\boldsymbol{L}^{(i)}$ is associated with the type of circuit characteristic. In the case of S-parameters, specifically S_{kl}, it is defined as (f stands for frequency)

$$S_{kl.L}^{(i)}(\mathbf{x},f) = S_{kl}(\mathbf{x}^{(i)},f) + \mathbf{G}_{kl}(\mathbf{x}^{(i)},f)\cdot(\mathbf{x}-\mathbf{x}^{(i)}) \quad (7)$$

where $\boldsymbol{x}^{(i)}$ is the current solution. In (7), $\boldsymbol{G}_{kl}(\boldsymbol{x}^{(i)},f)$ is the gradient of S_{kl} at $\boldsymbol{x}^{(i)}$. Sensitivity data is generated using finite differences, which entails n extra EM evaluations, where n is the decision variable space dimensionality. Several sparse sensitivity updating schemes were proposed, including adaptive Broyden updates [67], gradient variability tracking [36], or design relocation tracking [76]. We will explore some of these techniques in 3 as benchmark algorithms.

2.3. Variable-fidelity EM analysis

Variable-resolution analysis is employed in this study to accelerate EM-based optimization. Coarse-mesh EM analysis or other types of lower-fidelity models [55] have been used for quite a while for that purpose. However, two levels are predominantly considered (low-/-high-fidelity). Most often, the low-resolution model undergoes appropriate correction to serve as dependable predictor (space mapping [40], response correction [77,78]).

It can also be used within ML procedures [49] to facilitate parameter space exploration, or to boost the efficacy of surrogate model construction (e.g., co-kriging [79]). The main issue related to these approaches is that the low-resolution model must be properly selected regarding the associated trade-off between its cost and predictive power, which is not a trivial matter [71].

For illustration, Fig. 4 shows a dual-band power divider to be later used as a verification case study in Section 3, as well as its frequency characteristics evaluated using EM analysis of different resolutions. The model's mesh density is decided upon by means of the lines-per-wavelength (LPW) coefficient, which determines the mesh density of the EM model of the device in CST Microwave Studio (here, using the time-domain solver). The EM simulation time as a function of LPW has been visualized in Fig. 4(b), whereas Fig. 4(c) demonstrates the circuit S-parameters for different resolution levels. It can be noted that reducing LPW beyond nine leads to a severe distortion of the response. Consequently, LPW = 9 can be considered the lowest usable value. Meanwhile, LPW of 27 can be viewed as the high-fidelity representation as increasing discretization density further has essentially no effect on the frequency characteristics.

In the following, that lowest and the higher LPWs will be denoted as L_{min} and L_{max}, respectively. In this work, we employ the entire spectrum of resolutions L within the range $L_{min} \le L \le L_{max}$. The specific model management scheme will be elucidated in the next section.

The selection of the minimum and maximum model fidelity levels L_{min} and L_{max} is an important aspect of the proposed methodology. However, it should be emphasized that the selection process is complex, primarily because the appropriate values are problem dependent and vary considerably among real-world components. The selection process must take into account the trade-off between simulation cost and model accuracy. Some general rules may be formulated:

- The discretization of the low-fidelity should not be too coarse to avoid excessive response distortion, which may compromise the reliability of the design process,

1. Input parameters:
   - Initial design $\boldsymbol{x}^{(0)}$;
   - Objective function U;
   - Minimum and maximum model resolutions $L_{\min}$ and $L_{\max}$;
   - Control parameters: ε_{TR}, λ, $Q_{c.ming}$, $Q_{c.\max}$, $Q_{q.\min}$, $Q_{q.\max}$;
2. Set the iteration counter $i = 0$, and $L^{(i)} = L_{\min}$;
3. Evaluate circuit response $\boldsymbol{R}(\boldsymbol{x}^{(i)})$ at the discretization level $L^{(i)}$;
4. Evaluate circuit sensitivities $\boldsymbol{J}_R(\boldsymbol{x}^{(i)})$ at the discretization level L_{FD} (cf. (12));
5. Construct a linear model $\boldsymbol{L}^{(i)}(\boldsymbol{x}) = \boldsymbol{R}(\boldsymbol{x}^{(i)}) + \boldsymbol{J}_R(\boldsymbol{x}^{(i)})\cdot(\boldsymbol{x} - \boldsymbol{x}^{(i)})$;
6. Obtain the design $\boldsymbol{x}^{(i+1)}$ by solving (4);
7. Evaluate circuit response $\boldsymbol{R}(\boldsymbol{x}^{(i+1)})$ at the discretization level $L^{(i)}$;
8. Update trust-region size parameter $d^{(i)}$ [77];
9. **if** $U(\boldsymbol{x}^{(i+1)}) < U(\boldsymbol{x}^{(i)})$
   - Compute convergence indicator $Q_c^{(i)}$ using (8);
   - Compute quality indicator $Q_q^{(i)}$ using (9);
   - Compute $L^{(i+1)}$ using (11);
   - Set $i = i + 1$;

   end
10. **if** $||\boldsymbol{x}^{(i+1)} - \boldsymbol{x}^{(i)}|| < \varepsilon_{TR}$ OR $d^{(i)} < \varepsilon_{TR}$
    - Go to 11;

    else
    - Go to 4;

    end
11. END.

Fig. 8. Pseudocode of the proposed procedure. The circuit characteristics are marked as $\boldsymbol{R}(\boldsymbol{x})$, whereas $\boldsymbol{J}_R(\boldsymbol{x})$ is the Jacobian matrix.

- The discretization of the low-fidelity should not be excessively fine, as this would unnecessarily increase the computational cost and reduce the benefits of using a low-fidelity model,
- The discretization of the fine-fidelity model should not be excessively fine, as this would unnecessarily increase the computational cost of the design process without providing any improvement in accuracy.

In practice, the fidelity range is established through experience-guided visual inspection of the model responses. This procedure involves (see Fig. 4):

1. Simulation of a family of model responses at different model resolution levels at the initial design. As a rule of thumb, when the parameter LPW of CST Microwave Studio is employed for setting the model resolution level, a recommended range is approximately 7–30,
2. Assessment of the relationship between model accuracy and simulation time for the considered design case (cf. Fig. 4(b)),
3. Identification of the coarsest discretization that preserves the essential features and trends of the response (cf. Fig. 4(c)) while providing a meaningful reduction in simulation time (cf. Fig. 4(b)).
4. Determination of the fine model resolution beyond which further refinement produces no significant changes in the model response (cf. Fig. 4(c)).

2.4. Model management strategy

The EM model resolution L is controlled during optimization within the range from $L_{\min}$ to $L_{\max}$ using a custom model management scheme described below. For demonstration, it is coupled with the TR routine introduced in Section 2.2. The goal is to expedite the search process without affecting its reliability. Towards this end, the following rules are to be observed:

- The lowest admissible resolution $L_{\min}$ should be used early in the optimization run to enable acceleration,
- The highest fidelity $L_{\max}$ must be applied at the conclusion of the optimization run to secure evaluation quality,
- The resolution adjustment should involve factors such as the convergence status, here, measured by $||\mathbf{x}^{(i+1)} - \mathbf{x}^{(i)}||$;
- The resolution changes should also depend on the quality of the current design, e.g., the value of the merit function $U(\mathbf{x}^{(i)})$; in particular, evaluating poor designs at lower resolution levels allows reducing the waste of computational resources,
- For stability, the resolution adjustments should be monotonic w.r.t. the mentioned factors.

Recall that the TR algorithm is aborted if $||\mathbf{x}^{(i+1)} - \mathbf{x}^{(i)}|| < \varepsilon_{TR}$ (cf. Fig. 3). The threshold $\varepsilon_{TR} = 10^{-3}$ in the verification studies discussed in Section 3. The model adjustment strategy uses the convergence and quality indicators $Q_c^{(i)}$ and $Q_q^{(i)}$ formulated as

$$Q_c^{(i)} = \log\left(\frac{||\mathbf{x}^{(i+1)} - \mathbf{x}^{(i)}||}{\varepsilon_{TR}}\right) \tag{8}$$

$$Q_q^{(i)} = U\left(\mathbf{x}^{(i)}\right) \tag{9}$$

We also need additional control parameters introduced in Fig. 5. According to these, the model resolution starts increasing when $Q_c^{(i)} < Q_{c.\max}$ and reaches the maximum value w.r.t. this criterion when $Q_c^{(i)} > Q_{c.\min}$. Similarly, the resolution start increasing when $Q_q^{(i)} < Q_{q.\max}$, and reaches the maximum value w.r.t. the quality-related when $Q_q^{(i)} > Q_{q.\min}$. The design problems considered in Section 3 are formulated to improve in-band reflection and port isolation (the minimax objective function defined similarly as shown in Fig. 2). Therefore, $Q_{q.\min}$ is set to –10 dB and $Q_{q.\max} = 0$ dB because the expected objective function values at satisfactory designs are at the level lower than –10 dB.

The control parameters of the model management scheme influence the algorithm's performance, and their recommended values are based on the practical considerations. The parameter $Q_{c.\min}$ allows assessing whether the optimization process is close to convergence. Hence, its recommended value is 1, which corresponds to the optimization procedure being one decade from convergence on a logarithmic scale. While

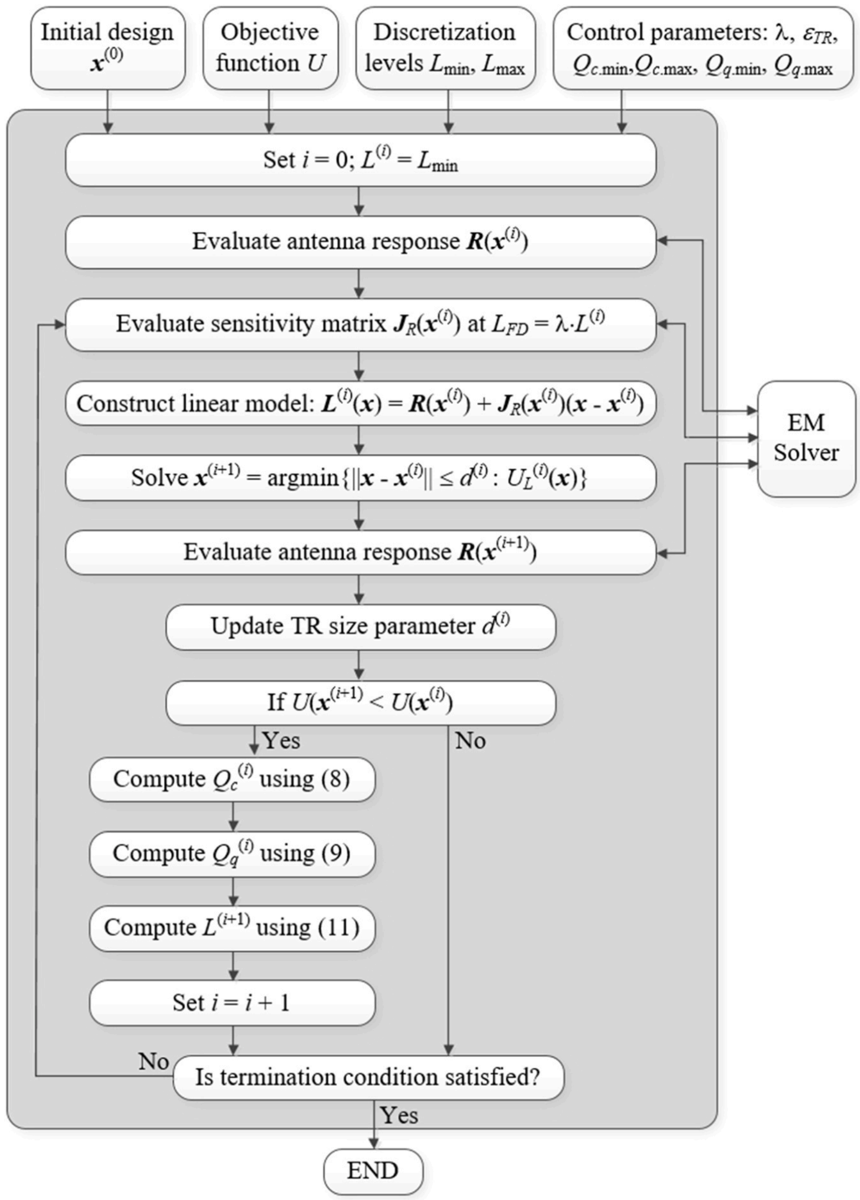

Fig. 9. Flow diagram of the proposed variable-fidelity procedure.

the parameter $Q_{c.max}$ allows assessing whether the optimization process is away from convergence, and its recommended value equals 3. Increasing $Q_{c.min}$ would lead to the premature use of the high-fidelity model, which would significantly reduce the efficiency of the entire procedure. While increasing $Q_{c.max}$ would lead to the prolonged use of the low-fidelity model, which could reduce the accuracy of the optimal design

The quality-related parameters are problem-dependent. We recommend (see Fig. 5) using $Q_{q.min} = 0$ dB and $Q_{q.max} = -15$ dB for a constrained objective function defined to minimize in-band reflection/isolation. If other arrangements need to be applied, a designer needs to set the quality-related parameters based on what is considered acceptable or unacceptable for the specific design objectives in question.

One final component of the model management procedure is the transition function T defined as follows:

$$T(q, q_{\min}, q_{\max}) = \begin{cases} 1 & \text{if} \quad q < q_{\min} \\ \dfrac{q_{\max} - q}{q_{\max} - q_{\min}} & \text{if} \quad q_{\min} \le q \le q_{\max} \\ 0 & \text{if} \quad q > q_{\max} \end{cases} \tag{10}$$

Using (8), (9), and (10), we are now able to provide a formula for adjusting the model fidelity $L^{(i)}$ at the end of the ith iteration. We have

$$L^{(i+1)} = \max\left\{L^{(i)}, L_{\min} + (L_{\max} - L_{\min}) T\left(Q_c^{(i)}, Q_{c.\ \min}, Q_{c.\ \max}\right) T\left(Q_q^{(i)}, Q_{q.\ \min}, Q_{q.\ \max}\right)\right\} \tag{11}$$

As mentioned earlier, $L^{(0)} = L_{min}$, i.e., the search starts using the lowest usable resolution. According to (11), the EM analysis fidelity is a function of the convergence and design quality indicators. If a satisfactory design is attainable, i.e., there is a parameter vector $\mathbf{x}$ for which $Q_q(\mathbf{x}) < Q_{q.min}$, then the model resolution will eventually increase to L_{max} when the algorithm approaches convergence (that is, when $Q_c(\mathbf{x}) < Q_{c.min}$). The latter ensures that the high-fidelity simulation is

Table 1
Control parameters of the presented algorithm.

Purpose	Symbol	Description	Default value
Variable-fidelity model management scheme	$Q_{c.\min}$	Determination whether optimization is near convergence	1
	$Q_{c.\max}$	Determination whether the process is away from convergence	3
	$Q_{q.\min}$	Determination whether the design quality is satisfactory	Problem dependent
	$Q_{q.\max}$	Determination whether the design quality is poor	Problem dependent
Model resolution	$L_{\min}$	The lowest model fidelity	Problem dependent
	$L_{\max}$	The highest model fidelity	Problem dependent
	λ	Setting the resolution for sensitivity evaluation $L_{FD} = \max\{L_{\min}, \lambda L(i)\}$	2/3
Algorithm termination	ε_{TR}	Termination threshold	10^{-3}

employed at the final optimization stages. On the other hand, if a satisfactory design is not reachable in terms of the quality indicator Q_q, then the high-fidelity model will not be used. It should be reiterated that the model management strategy proposed here is simpler than the multi-fidelity scheme of [72]. Recall that the latter requires re-starting the search if the high-fidelity model ($L_{\max}$) was not employed when close to convergence.

A visualization of the quantities used to control the EM analysis resolution and the management scheme can be found in Fig. 6. A visualization of the functional dependence between the convergence and quality indicators and the model resolution (parameter L) has been provided in Fig. 7.

Further acceleration can be achieved by evaluating the circuit response sensitivities within the TR scheme at the resolution level which is lower than $L^{(i)}$. More specifically, finite differentiation is carried out using the resolution L_{FD}, established as

$$L_{FD} = \max\{L_{\min}, \lambda L^{(i)}\} \tag{12}$$

The resolution-governing parameter in (12) is $\lambda = 2/3$ as recommended in [72]. Clearly, EM simulation at the resolution level L_{FD} is less accurate than at the level $L^{(i)}$; however, as the models of different fidelities are evaluated using the same procedure (here, FDTD), they are normally well correlated even if their misalignment is noticeable in absolute terms.

2.5. Complete optimization algorithm

Fig. 8 provides the pseudocode of the algorithm incorporating the management strategy of Section 2.4. For auxiliary explanation, Fig. 9 presents the block diagram of the framework. The only control parameters are the termination threshold ε_{TR} and the multiplier λ for setting up the resolution level L_{FD} for finite differentiation (cf. (12)). Their default values are 10^{-3} and 2/3, accordingly. The bounds for convergence and quality indicators have been discussed in Section 2.3, see also Fig. 5. The resolution levels $L_{\min}$ and $L_{\max}$ are problem dependent. As discussed in Section 2.3, these are determined through initial simulations, and a visual inspection of the circuit characteristics. All of the controls parameters are juxtaposed in Table 1.

3. Numerical results

The variable-resolution algorithm presented in Section 2 is showcased here using three microstrip circuits, a power divider, an impedance matching transformer, and a compact branch-line coupler. The performance of our procedure is juxtaposed against the baseline TR routine of Section 2.2, two accelerated versions [76,80], as well as the multi-fidelity technique of [72]. The test cases have been outlined in Section 3.1, whereas the benchmark methods are summarized in Section 3.2. Comparative experiments involve multiple optimization runs starting from randomly selected parameter vectors. The performance metrics, the optimization cost and design dependability measured using the merit function value at the final designs. The outcomes are collected in Section 3.3 and interpreted in Section 3.4. Section 3.5 covers prototyping and measurements of selected designs optimized using our

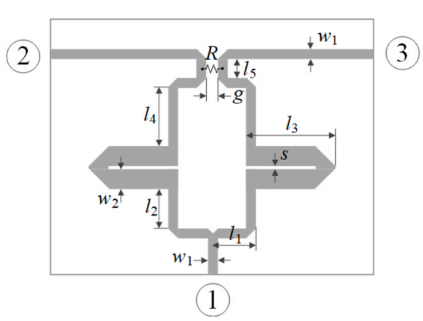

(a)

Substrate	AD250 (ε_r = 2.5, h = 0.81 mm, tanδ = 0.0018)
Design variables	$\boldsymbol{x} = [l_1\ l_2\ l_3\ l_4\ l_5\ s\ w_2]^T$
Other parameters	w_1 = 2.2; g = 1 mm
Design objectives	• Operating frequencies: f_1 = 2.4 GHz and f_2 = 3.8 GHz; • Input and output matching $\|S_{11}\|$, $\|S_{22}\|$, $\|S_{33}\|$, to be minimized within the frequency bands [f_1 – 100 MHz, f_1 + 100 MHz] and [f_2 – 100 MHz, f_2 + 100 MHz]; • Port isolation $\|S_{23}\|$ to be minimized within the frequency bands [f_1 – 100 MHz, f_1 + 100 MHz] and [f_2 – 100 MHz, f_2 + 100 MHz];

(b)

Variable-resolution EM model setup		
Lowest-fidelity model	$L_{\min}$	9
	Simulation time [s]	52
High-fidelity model	$L_{\max}$	27
	Simulation time [s]	360

(c)

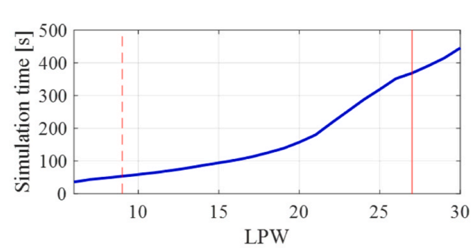

(d)

Fig. 10. Circuit I: dual-band power divider [81]: (a) parameterized circuit geometry (100-ohm resistor marked as R), (b) essential parameters and design goals, (c) variable-resolution model setup, (d) dependence between LPW and the EM analysis time. Vertical lines mark $L_{\min}$ (- - -) and $L_{\max}$ (—) considered for the circuit.

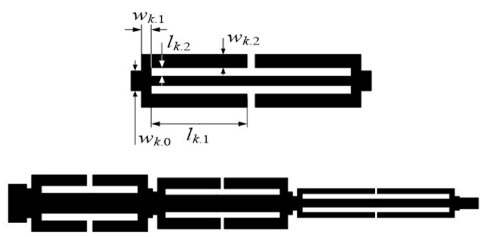

(a)

Substrate	RF-35 ($\varepsilon_r = 3.5$, $h = 0.76$ mm, $\tan\delta = 0.0027$)
Design variables	$\boldsymbol{x} = [l_{1.1}\ l_{1.2}\ w_{1.1}\ w_{1.2}\ w_{1.0}\ l_{2.1}\ l_{2.2}\ w_{2.1}\ w_{2.2}\ w_{2.0}\ l_{3.1}\ l_{3.2}\ w_{3.1}\ w_{3.2}\ w_{3.0}]^T$
Other parameters	-
Design objectives	• Operating bandwidth: $[f_1\ f_2] = [1.5\ 4.5]$ GHz; • Input matching $\|S_{11}\|$ to be minimized the target band $[f_1\ f_2]$;

(b)

Variable-resolution EM model setup		
Lowest-fidelity model	$L_{\min}$	7
	Simulation time [s]	33
High-fidelity model	$L_{\max}$	23
	Simulation time [s]	140

(c)

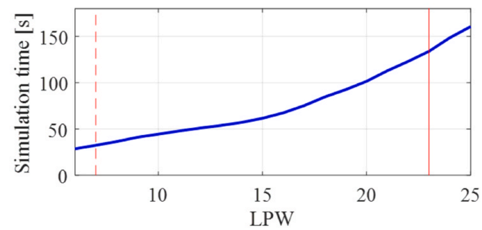

(d)

Fig. 11. Circuit II: three-section 50-to−100-ohm impedance matching transformer [82]: (a) parameterized circuit geometry (unit cell and the three-section circuit), (b) essential parameters and design goals, (c) variable-resolution model setup, (d) dependence between LPW and the EM analysis time. Vertical lines mark $L_{\min}$ (- - -) and $L_{\max}$ (—) considered for the circuit.

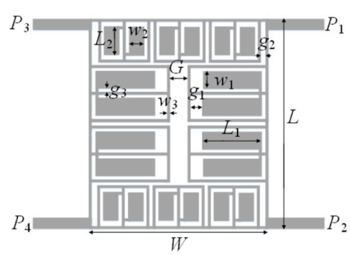

(a)

Substrate	FR4 ($\varepsilon_r = 4.4$, $h = 1.0$ mm)
Design variables	$\boldsymbol{x} = [G\ g_1\ g_2\ g_3\ w_1\ w_3\ L_1\ L_2]^T$
Other parameters	$L = 4w_1 + 10w_3 + 15g_3 + 2L_2$, $W = 4w_3 + 2L_1 + G + 2g_1 + 2g_3$
Design objectives	• Operating bandwidth: $[f_1\ f_2] = [0.95\ 1.05]$ GHz; • Input matching $\|S_{11}\|$ and port isolation $\|S_{41}\|$ to be minimized the target band $[f_1\ f_2]$; • Equal power split to be preserved at $f_0 = 1$ GHz.

(b)

Variable-resolution EM model setup		
Lowest-fidelity model	$L_{\min}$	12
	Simulation time [s]	120
High-fidelity `model	$L_{\max}$	24
	Simulation time [s]	310

(c)

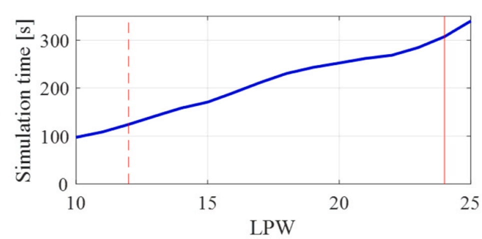

(d)

Fig. 12. Circuit III: compact branch-line coupler [83]: (a) parameterized circuit geometry, (b) essential parameters and design goals, (c) variable-resolution model setup, (d) dependence between LPW and the EM analysis time. Vertical lines mark $L_{\min}$ (- - -) and $L_{\max}$ (—) considered for the circuit.

method.

3.1. Test cases

Figs. 10–12 show the verification circuits, their essential parameters, the variable-resolution model setup, and the dependence of the EM simulation time on the model resolution. The EM models are prepared in CST Microwave Studio and evaluated by means of the time-domain solver.

Circuit I (a dual-band power divider) is to be optimized for minimum input and output matching and port isolation, at the two bands [2.3 2.5] GHz and [3.7 3.9] GHz. Circuit II (a 50-to−100-ohm impedance matching transformer) is optimized for best matching within the frequency range 1.5 GHz to 4.5 GHz. Circuit III (a compact branch-line coupler) is optimized for minimum in-band matching and port isolation at the operating band 0.95 GHz to 1.05 GHz, while preserving equal power split ratio at $f_0 = 1$ GHz. It should be reiterate that the ratio of the simulation time between the high- and the lowest-resolution models is close to seven for Circuit I, over four for Circuit II, and about 2.5 for Circuit III, which indicates that considerable savings may be achieved due to the variable-resolution approach.

3.2. Experimental setup. Benchmark algorithms

The algorithm introduced in Section 2 is juxtaposed against several benchmark methods described in Fig. 13. These include the baseline TR procedure discussed in Section 2.2, which solely employs the high-fidelity EM model, two accelerated versions [76,80], both using sparse

Algorithm	Characterization
Algorithm 1	• Reference TR algorithm as described in Section 2.2; • Optimization process exclusively based on high-fidelity EM simulations (i.e., at the discretization level of $L_{\max}$ for the respective structures).
Algorithm 2	• Expedited version of the reference algorithm using solely high-fidelity EM simulations [77]; • Main acceleration mechanism: suppressing some of the finite-differentiation (FD)-based Jacobian updates, based upon the magnitude of the relative design change with respect to the current TR region size; • Design change between consecutive iterations is assessed by the selection factors $$\varphi_k^i = \left\| x_k^{(i+1)} - x_k^{(i)} \right\| \Big/ d_k^{(i)}, \quad k = 1, \ldots, n,$$ where $x_k^{(i)}$, $x_k^{(i+1)}$ stand for the kth elements of the parameter vectors $\boldsymbol{x}^{(i)}$, $\boldsymbol{x}^{(i+1)}$ of the two most recent iterations, respectively, and $d_k^{(i)}$ refers to the kth entry of the TR region size vector $\boldsymbol{d}^{(i)}$; • For a given parameter k, if φ_k^i is lower than a user-specified threshold, FD is not performed, and the previous value of the appropriate Jacobian column is retained; • To enforce the update once in few iterations, the optimization history is inspected. The maximum allowable number of iterations N without the update is the algorithm control parameter, here, set to $N = 3$ as recommended in [77].
Algorithm 3	• Expedited version of the reference TR algorithm involving sensitivity updating formulas, also exclusively based on high-fidelity EM simulations; • For the directions that are sufficiently well aligned with the most recent design relocation, the Jacobian matrix is updated with a rank-one Broyden formula (BF) rather than through FD. The following alignment factors are defined $$\gamma_k^{(i)} = \left\| \boldsymbol{h}^{(i)T} \boldsymbol{e}^{(k)} \right\| / \left\| \boldsymbol{h}^{(i)} \right\|, \quad k = 1, \ldots, n,$$ where $\boldsymbol{e}^{(k)}$ corresponds to the standard basis vectors (i.e., $\boldsymbol{e}^{(k)}$ contains only zeros except for 1 on the k-th position), and $\boldsymbol{h}^{(i+1)} = \boldsymbol{x}^{(i+1)} - \boldsymbol{x}^{(i)}$. • For a given parameter k, if $\gamma_k^{(i)}$ is larger than a user-defined threshold $\gamma_{\min}$, the appropriate Jacobian portion is updated with BF. The algorithm control parameter $0 \le \gamma_{\min} \le 1$ can be used to govern the trade-offs between the computational savings and the design quality. Here, $\gamma_{\min} = 0.9$ is used as recommended in [81].
Algorithm 4	• Expedited version of the reference TR algorithm involving multi-fidelity simulation models [62]; • The model fidelity is adjusted within the range from $L_{\min}$ to $L_{\max}$ determined the same way as in the algorithm proposed here; • Model management strategy is exclusively based on convergence indicators $$L^{(i+1)} = \begin{cases} L_{\min} \quad \text{if} \quad Q^{(i)}(\varepsilon_x, \varepsilon_U) \le M \\ \max\left\{ L^{(i)}, L_{\min} + \left(L_{\max} - L_{\min}\right)\left[1 - \dfrac{\log(Q^{(i)}(\varepsilon_x, \varepsilon_U))}{\log M}\right] \right\} \end{cases}$$ where $$Q^{(i)}(\varepsilon_x, \varepsilon_U) = \max\left\{ \frac{\varepsilon_x}{\| \boldsymbol{x}^{(i+1)} - \boldsymbol{x}^{(i)} \|}, \frac{\varepsilon_U}{\| U_P(\boldsymbol{x}^{(i+1)}) - U_P(\boldsymbol{x}^{(i)}) \|} \right\}$$ and M is threshold for initiating model fidelity increase; ε_x and ε_U are termination thresholds for convergence in argument and objective function values; • Finite differentiation is executed at lower fidelity as in (12); • There is no guarantee that the optimization process will end up at high-fidelity level ($L_{\max}$): therefore, upon convergence, the optimization process is restarted using $L_{\max}$ to ensure sufficient accuracy [72].

Fig. 13. Benchmark methods used to validate the variable-resolution algorithm proposed in this work.

sensitivity updates, and the multi-fidelity approach of [72]. A remark should be made that presented optimization framework is a local gradient-based design technique, and therefore it is compared against algorithms belonging to the same class. An alternative direction in microwave design involves machine-learning-based surrogate-assisted approaches. However, methods of this class require training dedicated models before any design tasks can be carried out. This training stage is computationally demanding due to the high-nonlinearity of the components' responses and the broad parameter ranges, and it typically by far exceeds the cost associated with our methodology. Moreover, surrogate-based optimization constitutes a fundamentally different category of techniques and is outside the scope of the present work.

All algorithms have been run 10 times initiated from randomly selected starting points. This setup allows for gathering meaningful information and diminishing bias related to a specific starting point selection.

The operation of the procedure is evaluated based on the following factors:

Table 2
Results for Circuit I.

Algorithm	Performance figure				
	Cost[a]	Cost savings[b]	Objective function value[c]	Objective function degradation[d]	Standard deviation of the objective function[e]
Algorithm 1 (Conventional TR search)	91.9	–	–17.2 dB	–	1.8 dB
Algorithm 2 (Accelerated TR search [76])	60.6	34%	–17.7 dB	–0.5 dB	3.8 dB
Algorithm 3 (Accelerated TR search [80])	72.4	21%	–16.9 dB	0.3 dB	3.7 dB
Algorithm 4 (Multi-fidelity [72])	31.7	66%	–17.2 dB	0.0 dB	1.6 dB
Variable-resolution (this work)	23.7	74%	–16.7 dB	0.5 dB	1.7 dB

[a] Number of equivalent high-fidelity EM simulations averaged over 10 algorithm runs.
[b] Relative computational savings in percent w.r.t. the reference algorithm.
[c] Objective function value averaged over 10 algorithm runs.
[d] Degradation of the objective function value w.r.t. the baseline algorithm in dB, averaged over 10 algorithm runs.
[e] Standard deviation of the objective function value in dB computed for the set of 10 algorithm runs.

Table 3
Results for Circuit II.

Algorithm	Performance figure				
	Cost[a]	Cost savings[b]	Objective function value[c]	Objective function degradation[d]	Standard deviation of the objective function[e]
Algorithm 1 (Conventional TR search)	123.8	–	–20.7 dB	–	1.1 dB
Algorithm 2 (Accelerated TR search [76])	79.3	36%	–20.7 dB	0 dB	0.7 dB
Algorithm 3 (Accelerated TR search [80])	59.5	52%	–20.3 dB	0.4 dB	1.2 dB
Algorithm 4 (Multi-fidelity [72])	78.3	37%	–19.3 dB	1.4 dB	1.8 dB
Variable-resolution (this work)	60.6	51%	–19.3 dB	1.4 dB	1.9 dB

[a] Number of equivalent high-fidelity EM simulations averaged over 10 algorithm runs.
[b] Relative computational savings in percent w.r.t. the reference algorithm.
[c] Objective function value averaged over 10 algorithm runs.
[d] Degradation of the objective function value w.r.t. the baseline algorithm in dB, averaged over 10 algorithm runs.
[e] Standard deviation of the objective function value in dB computed for the set of 10 algorithm runs.

Table 4
Results for Circuit III.

Algorithm	Performance figure							
	Cost[a]	Cost savings[b]	Maximum in-band $\|S_{11}\|$, $\|S_{41}\|$[c]	Degradation of maximum in-band $\|S_{11}\|$, $\|S_{41}\|$[d]	Std of the objective function[e]	Power split ratio[c]	Degradation of the power split ratio[f]	Std of the power split ratio[g]
Algorithm 1 (Conventional TR search)	85.1	-	–16.3 dB	-	3.3 dB	0.1 dB	-	0.2 dB
Algorithm 2 (Accelerated TR search [76])	70.0	18%	–16.8 dB	–0.5 dB	0.8 dB	0.1 dB	0 dB	0.1 dB
Algorithm 3 (Accelerated TR search [80])	38.1	55%	–16.0 dB	0.3 dB	3.8 dB	0.3 dB	0.2 dB	0.4 dB
Algorithm 4 (Multi-fidelity [72])	53.7	37%	–13.6 dB	2.7 dB	2.4 dB	0.4 dB	0.3 dB	0.5 dB
Variable-resolution (this work)	33.6	61%	–15.0 dB	1.3 dB	1.9 dB	0.3 dB	0.2 dB	0.4 dB

[a] Number of equivalent high-fidelity EM simulations averaged over 10 algorithm runs.
[b] Relative computational savings in percent w.r.t. the reference algorithm.
[c] The value averaged over 10 algorithm runs.
[d] Degradation of the maximum in-band $|S_{11}|/|S_{41}|$ w.r.t. the baseline algorithm in dB, averaged over 10 algorithm runs.
[e] Standard deviation of the maximum in-band $|S_{11}|/|S_{41}|$ in dB computed for the set of 10 algorithm runs.
[f] Degradation of the power split ratio w.r.t. the baseline algorithm in dB, averaged over 10 algorithm runs.
[g] Standard deviation of the power split ratio in dB computed for the set of 10 algorithm runs.

- The optimization cost concerning the equivalent number of high-fidelity EM analyses of the device of interest,
- Reliability quantified using the mean value of the merit function over ten algorithm runs performed,
- Result repeatability estimated using the standard deviation of the merit function.

As mentioned earlier, the initial designs are assigned randomly, which means that the optimized parameter vectors may be associated with different local solutions. Consequently, the objective function's standard deviation is unlikely to be zero, and repeatability comparisons should be done with respect to the standard deviation of the baseline algorithm instead of the zero value.

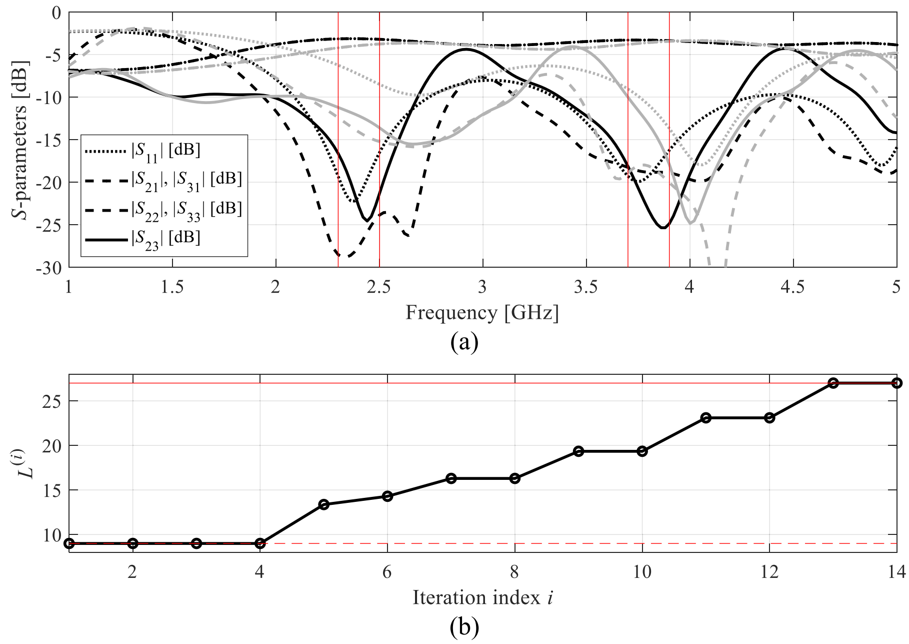

Fig. 14. Circuit I: (a) S-parameters versus frequency for the selected run of the presented algorithm: (- - -) initial design, (—) optimized design; target bands denoted using the vertical lines; (b) history of the model resolution; horizontal lines mark ($L_{\min}$ (- - -) and $L_{\max}$ (—).

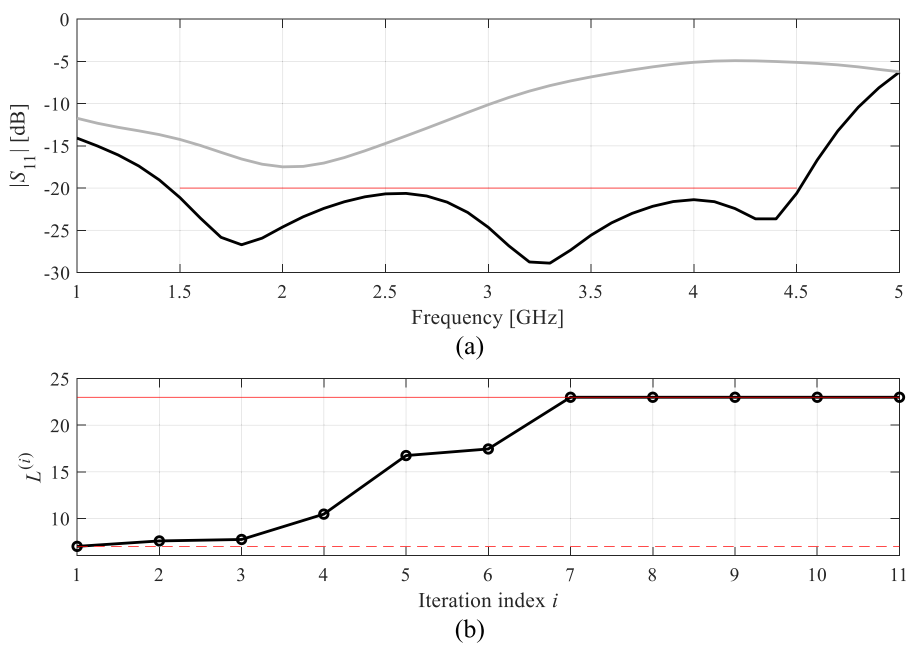

Fig. 15. Circuit II: (a) S-parameters versus frequency for the selected run of the presented algorithm: (- - -) initial design, (—) optimized design; target band denoted using the vertical lines; (b) history of the model resolution; horizontal lines mark ($L_{\min}$ (- - -) and $L_{\max}$ (—).

3.3. Results

Tables 2 through 4 gather numerical results obtained for Circuits I through III. Meanwhile, Figs. 14–16 show—for chosen runs of the presented algorithm—the EM-evaluated frequency responses along with the evolution of the model resolution. The data in Tables 2–4 consists of the mean values of the computational cost and merit function values, and their standard deviations, acquired during ten separate runs of each procedure. The expenses are given concerning the number of high-fidelity EM analyses, computed considering the actual simulation times of EM models of different resolutions.

3.4. Discussion

Using the data collected in Tables 2, 3, and 4, the operation of the presented variable-resolution algorithm is analyzed and compared to the procedures included in the benchmark set. Regarding cost efficiency, the presented methodology enables significant acceleration as over the baseline gradient-based routine (Algorithm 1). The savings exceed 74% for Circuit I, 51% for Circuit II, and 61% for Circuit III. As expected, the speedup is to a certain extent correlated with high-to-low model time evaluation ratio, which is about seven for Circuit I, about four for Circuit I, and slightly less than three for Circuit III.

The efficacy of the procedure considered is also significantly boosted

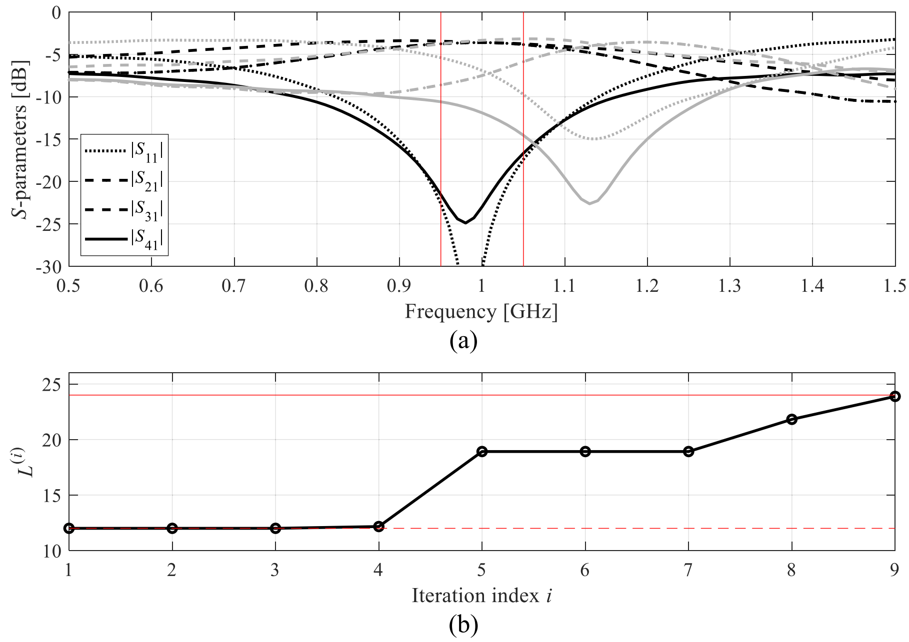

Fig. 16. Circuit III: (a) *S*-parameters versus frequency for the selected run of the presented algorithm: (- - -) initial design, (—) optimized design; target band denoted using the vertical lines; (b) history of the model resolution; horizontal lines mark ($L_{\min}$ (- - -) and $L_{\max}$ (—).

over the expedited TR routines (Algorithms 2 and 3), except for Algorithm 3 and Circuit II. Therein, the speedup achieved by Algorithm 3 is essentially the same as for our procedure. The average savings for Algorithms 2/3 are 28 % for Circuit I versus 74 % for the proposed algorithm. The corresponding numbers for Circuit II are 44 and 51 %, and 37 and 61 % for Circuit III.

It is also interesting to compare our methodology and the multi-fidelity approach of [72] (Algorithm 4). At can be observed, it is consistently faster for all considered test cases (74 versus 66 % savings for Circuit I, 51 versus 37 % for Circuit II, and 61 versus 37 % for Circuit III). A possible reason is that the algorithm introduced in this work employs an additional degree of freedom for model revolution adjustment, which is design quality. One should also remember that the procedure of [72] is more complex to implement than the technique presented here.

In terms of reliability, our methodology leads to a certain quality degradation, which is, however, only 0.5 dB on the average for Circuit I, slightly more than 1 dB for Circuit II, and about 1.3 dB for Circuit III (all regarding the baseline Algorithm 1). Meanwhile, the degradation is comparable to the multi-fidelity algorithm [72] (Algorithm 4), yet slightly more pronounced than for Algorithms 2 and 3.

Solution consistency, measured using the standard deviation of the merit function value, is essentially the same as that for the presented method and the baseline algorithm (Algorithm 1) for Circuit I, only slightly worse for Circuit II, but better for Circuit III. Meanwhile, the accelerated TR procedures (Algorithms 2 and 3) are somehow inconsistent: their corresponding standard deviations are very high for Circuit I (over twice as high as for other techniques), and lower than the average for Circuit II. For Circuit III, Algorithm 2 performs much better than Algorithm 3 in terms of the average design quality and solution consistency. Finally, the standard deviation of the merit function is essentially the same for the proposed technique and multi-fidelity Algorithm 4, except Circuit III, where the proposed approach prevails.

In summary, the proposed variable-resolution procedure offers competitive computational savings with minor degradation of reliability. It is straightforward to implement and can be integrated with several iterative search procedures. Therefore, it might be perceived as an high-performance alternative to conventional gradient-based routines but also their accelerated versions, including a prior implementation of the multi-fidelity scheme [72]. Because our technique employs numerical derivatives (finite differentiation) at all algorithm iterations, further acceleration is possible. It can be achieved by combining it with sparse sensitivity updating strategies (e.g., [76,80]), which will be investigated as a part of the future work.

3.5. Experimental validation

For supplementary illustration, selected designs, specifically, those considered in Figs. 14 through 16 were fabricated and measured. In the case of Circuit II, the device was manufactured in a back-to-back configuration because of using a 50-ohm-compatible measurement setup. The pictures of the prototypes and EM-simulated and experimentally validated responses are provided in Fig. 17. The agreement between the datasets is very good. Only small discrepancies can be noticed, which are primarily due to fabrication imperfections and the effects of connectors.

4. Conclusion

This research developed an innovative approach to expedited design closure (tuning) of microwave passive circuits using variable-resolution electromagnetic simulation models. Our approach involves a management scheme, where the model resolution is controlled based on the convergence and quality indicators. The search process starts at the lowest admissible level. The resolution steadily increases as the algorithm converges, and the design quality improves. This two-criterial adjustment strategy prevents from wasting computational resources when away from a satisfactory solution, thereby yielding significant computational speedup. Extensive verification was carried out using several microstrip circuits, and several state-of-the-art local optimization algorithms, including a recently reported multi-fidelity method. Numerical results demonstrate considerable savings of up to 74 % that can be obtained over the baseline (single resolution) algorithm with only small deterioration of the design quality. The suggested technique has been also shown to outperform accelerated algorithms regarding computational efficiency, and comparable to these in terms of reliability. The approach presented here may be considered a high-performance alternative to traditional design closure procedures. It is

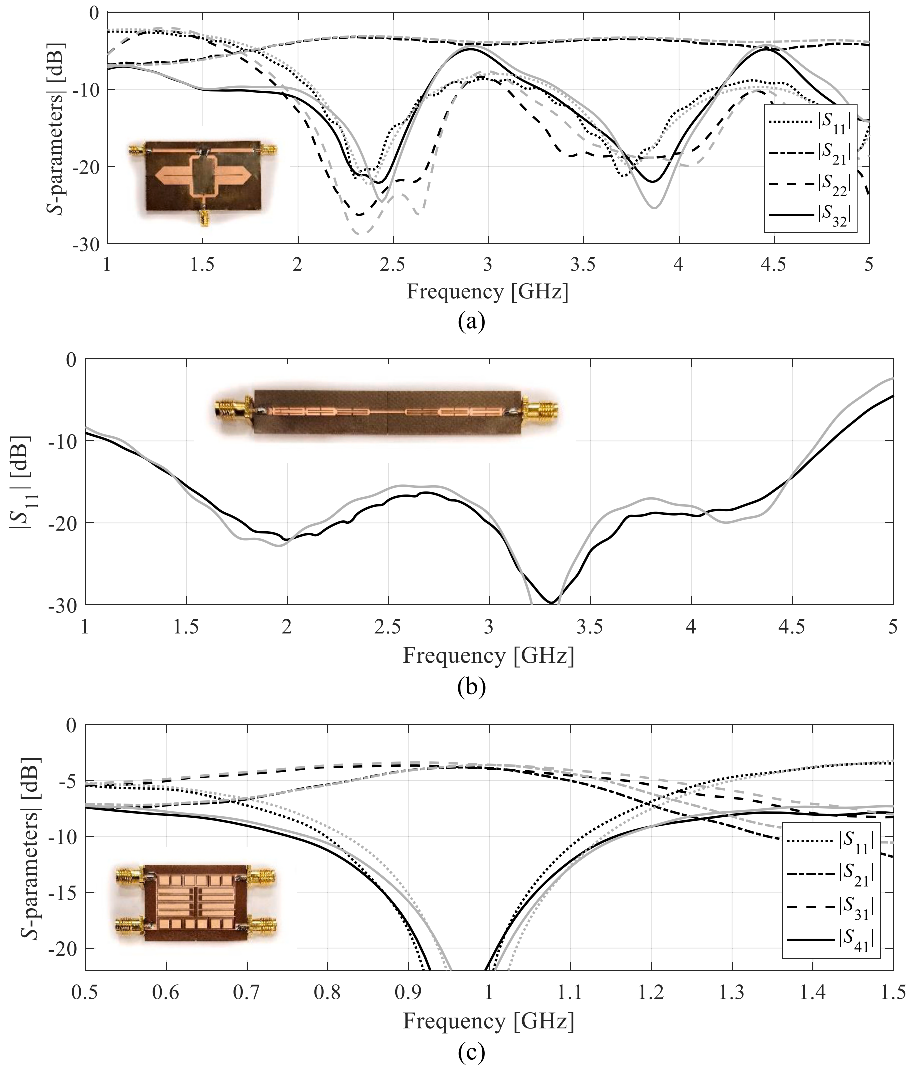

Fig. 17. Experimental validation of Circuits I through III for representative optimization runs shown in Figs. 14 through 16: (a) Circuit I, (b) Circuit II, (c) Circuit III. Measurement and EM-simulation shown using black and grey curves.

simple to implement and to integrate with diverse iterative search frameworks, particularly gradient-based algorithms. One of the aims of future research is the development of improved versions of the technique that ensure further acceleration, but also automation of the EM model resolution range determination. Furthermore, expanding the validation using a broader range of microwave structures to demonstrate the general applicability of the proposed methodology will be considered for future work.

CRediT authorship contribution statement

Anna Pietrenko-Dabrowska: Writing – review & editing, Visualization, Software, Project administration, Formal analysis. **Slawomir Koziel:** Writing – review & editing, Writing – original draft, Visualization, Validation, Supervision, Software, Resources, Project administration, Methodology, Investigation, Funding acquisition, Formal analysis, Data curation, Conceptualization.

Funding

This work is partially supported by the Icelandic Centre for Research (RANNIS) Grant 2410297 and by National Science Centre of Poland Grant 2024/55/B/ST7/01413.

Declaration of Competing Interest

The authors declare that they have no known competing financial interests or personal relationships that could have appeared to influence the work reported in this paper.

Acknowledgement

The authors would like to thank Dassault Systemes, France, for making CST Microwave Studio available.

Data availability

No data was used for the research described in the article.

References

[1] Z. Luo, L. Yang, T. Su, X. Zhu, R. Gómez-García, Single-ended and balanced flat-group-delay RF low-pass filters with input-quasi-reflectionless behavior for digital-communication systems, IEEE Trans. Microw. Theory Techn. 73 (1) (2025) 321–334.

[2] S. Lee, J. Lee, B. Lee, J. Lim, J. Han, J. Lee, K-band waveguide resonator bandpass filter structure with adjustable transmission zeros for producing various symmetric and asymmetric responses, IEEE Access. 13 (2025) 8664–8675.

[3] A. Kheirdoost, M. Haghparast, B. Ahmadi, M. Oldoni, Unitary condition, group delay and quality factor in microwave filters, IEEE J. Microw. 5 (2) (2025) 451–461.
[4] P. Li, J. Ren, Y. Chen, X. Ren, K.D. Xu, Y.Z. Yin, M. Shen, Design of low-cost single-layer 2-bit reflective programmable metasurface based on folded ground, IEEE Trans. Microw. Theory Techn. 71 (8) (2023) 3455–3465.
[5] B. Tegowski, A. Koelpin, A compact stacked SIW six-port junction, IEEE Microw. Wirel. Techn. Lett. 33 (5) (2023) 515–518.
[6] A. Noor, S. Koziel, Dual-polarized wideband bandpass metasurface-based filter, IEEE Ant. Wirel. Propag. Lett. 24 (1) (2024) 404–408.
[7] P. Li, W. Xu, D. Yang, An inversion design method for the radome thickness based on interval arithmetic, IEEE Ant. Wirel. Propag. Lett. 17 (4) (2018) 658–661.
[8] S. Chen, D. Ding, M. Yu, Y. Wang, R. Chen, Electro-thermal analysis of microwave limiter based on the time-domain impulse response method combined with physical-model-based semiconductor solver, IEEE Trans. Microw. Theory Techn. 68 (7) (2020) 2579–2589.
[9] H. Shen, F. Meng, Y. Wang, K. Ma, Self-packaged slow wave metal-integrated coplanar waveguide (MICPW) for compact branch-line coupler design, IEEE Trans. Comp. Pack. Manuf. Techn 15 (1) (2025) 196–205.
[10] Z. He, C. Liu, A compact high-efficiency broadband rectifier with a wide dynamic range of input power for energy harvesting, IEEE Microw. Wirel. Comp. Lett. 30 (4) (2020) 433–436.
[11] H. Xie, W.-J. Wu, W.-S. Zhao, W. Wang, A differential microwave sensor based on modified high-sensitivity substrate-integrated waveguide (SIW) for detecting glucose concentration in aqueous solution, IEEE Sens. J. 25 (10) (2025) 16998–17010.
[12] B. Gowrish, R.R. Mansour, A Novel bandwidth reconfigurable waveguide filter for aerospace applications, IEEE Microw. Wirel. Comp. Lett. 30 (6) (2020) 577–580.
[13] D. Psychogiou, R. Gómez-García, Compact substrate-integrated bandstop filters using double-resonant coaxial resonators, IEEE Microw. Wirel. Comp. Lett. 30 (10) (2020) 941–944.
[14] X. Tan, Y. Zhang, A compact rat-race coupler with widely tunable frequency- and power-dividing ratio, IEEE Microw. Wirel. Techn. Lett. 34 (1) (2024) 17–20.
[15] S. Kumari, P.K. Jain, M. Mahto, Study of a modified complementary electric split ring resonator-based metamaterial slow wave structure, IEEE Trans. Plasma Sc. 51 (8) (2023) 2205–2211.
[16] M. Malki, L. Yang, R. Gómez-García, Ku-band reflectionless single- and dual-band bandpass filters in groove gap waveguide, IEEE Trans. Microw. Theory Techn 73 (9) (2025) 5813–5827.
[17] Ahammad, A.I. Omi, M.H. Maktoomi, M.A. Maktoomi, P.K. Sekhar, On the design of a high band-ratio mid-section crossed dual-band branch-line coupler with arbitrary power division ratio using perturbation factor, IEEE Access. 13 (2025) 4609–4620.
[18] A.J. Alazemi, M.A. Koura, Optimization-based design of multi-band branch-line coupler with arbitrary and band-distinct power division ratios and phase differences, IEEE J. Microw. 5 (1) (2025) 224–239.
[19] M. Ahsan Halimi, I. Al-Naib, H. Attia, Multi-band microwave rectifiers for RF energy harvesting: a comprehensive review of design techniques and performance analysis, IEEE Access. 13 (2025) 140061–140078.
[20] M. Liu, et al., Multifunction reconfigurable phase shifter with independent 360° transmission and reflection phase tuning for multibit reconfigurable intelligent surface, IEEE Microw. Wirel. Techn. Lett. 35 (9) (2025) 1328–1331.
[21] T. Brown, P. Mojabi, Cascaded metasurface design using electromagnetic inversion with gradient-based optimization, IEEE Trans. Ant. Propag. 70 (3) (2022) 2033–2045.
[22] V. Gongal-Reddy, S. Zhang, C. Zhang, Q. Zhang, Parallel computational approach to gradient based EM optimization of passive microwave circuits, IEEE Trans. Microw. Theory Techn. 64 (1) (2016) 44–59.
[23] A. Afsari, A. Abbosh, Y. Rahmat-Samii, Quasi-gradient nonlinear simplex optimization method in electromagnetics, IEEE Access. 11 (2023) 59599–59611.
[24] X. Peng, L. Kong, X. Sun, H. Lyu, Design and analysis of optical receiving antenna for LED visible light communication based on Taguchi method, IEEE Access. 7 (2019) 186364–186377.
[25] X. Jia, G. Qin, C. Li, Improved hybrid real-binary PSO using modified learning and restarting methods for planar microwave absorber designs, IEEE Access. 11 (2023) 15505–15513.
[26] Z.C. Zhang, F. Hou, D.W. Wang, J. Liu, W.S. Zhao, PSO-algorithm-assisted design of compact SSPP transmission line, IEEE Microw. Wirel. Techn. Lett. 33 (3) (2023) 247–250.
[27] F. Güneş, A. Uluslu, P. Mahouti, Pareto optimal characterization of a microwave transistor, IEEE Access. 8 (2020) 47900–47913.
[28] P. Singh, S.S. Panda, J.C. Dash, B. Riscob, S.K. Pathak, R.S. Hegde, Rapid multi-objective antenna synthesis via deep neural network surrogate-driven evolutionary optimization, IEEE J. Multiscale Multiphysics Comp. Techn. 10 (2025) 151–159.
[29] Z. Zhang, B. Liu, Y. Yu, M. Imran, Q.S. Cheng, M. Yu, A surrogate modeling space definition method for efficient filter yield optimization, IEEE Microw. Wirel. Techn. Lett. 33 (6) (2023) 631–634.
[30] P. Manfredi, Probabilistic uncertainty quantification of microwave circuits using Gaussian processes, IEEE Trans. Microw. Theory Techn. 71 (6) (2023) 2360–2372.
[31] W. Na, K. Liu, W. Zhang, F. Feng, J. Zhang, H. Xie, D. Jin, Q.J. Zhang, Advanced EM optimization using adjoint-sensitivity-based multifeature surrogate for microwave filter design, IEEE Microw. Wirel. Techn. Lett. 34 (1) (2024) 1–4.
[32] S. Koziel, F. Mosler, S. Reitzinger, P. Thoma, Robust microwave design optimization using adjoint sensitivity and trust regions, Int. J. RF Microw. CAE 22 (1) (2012) 10–19.
[33] S. Ji, S. HuYan, L. Du, X. Xu, J. Zhao, Efficient adjoint-based shape optimization method for the inverse design of microwave components, IEEE Trans. Microw. Theory Techn. 73 (1) (2025) 494–504.
[34] F. Feng, J. Xue, J. Zhang, M. Li, W. Liu, Q.J. Zhang, Concise and compatible MOR-based self-adjoint EM sensitivity analysis for fast frequency sweep, IEEE Trans. Microw. Theory Techn. 71 (9) (2023) 3829–3840.
[35] A. Pietrenko-Dabrowska, S. Koziel, Computationally-efficient design optimization of antennas by accelerated gradient search with sensitivity and design change monitoring, IET Microw. Ant. Prop. 14 (2) (2020) 165–170.
[36] S. Koziel, A. Pietrenko-Dabrowska, Reliability enhancement of EM-based tuning of microwave components using regularized operating band scanning, Sc. Rep. 15 (paper 28000) (2025).
[37] J. Fu, J. Jin, J. Yang, Z. Liu, J. Qian, H. Lin, Feature-assisted neural network surrogate-based multiphysics optimization for microwave filters, IEEE Microw. Wirel. Techn. Lett. 34 (5) (2024) 474–477.
[38] A. Pietrenko-Dabrowska, S. Koziel, Q.J. Zhang, Cost-efficient two-level modeling of microwave passives using feature-based surrogates and domain confinement (paper no), Electronics 12 (17) (2023) 3560.
[39] B. Liu, L. Xue, H. Fan, Y. Ding, M. Imran, T. Wu, An efficient and general automated power amplifier design method based on surrogate model assisted hybrid optimization technique, IEEE Trans. Microw. Theory Techn. 73 (2) (2025) 926–937.
[40] M. Li, Q.J. Zhang, F. Feng, J. Xue, W. Liu, J. Jin, J. Zhang, W. Zhang, Advanced mesh space mapping approach with fast coarse mesh models comprising sharpening structural processing and mesh deformation, IEEE Trans. Microw. Theory Techn. 72 (3) (2024) 1578–1590.
[41] D. Gorissen, K. Crombecq, I. Couckuyt, T. Dhaene, P. Demeester, A surrogate modeling and adaptive sampling toolbox for computer based design, J. Mach. Learn. Res. 11 (2010) 2051–2055.
[42] S. Marelli and B. Sudret, UQLab: a framework for uncertainty quantification in Matlab, in The 2nd Int. Conf. on Vulnerability and Risk Analysis and Management (ICVRAM 2014), University of London, UK, July 13-15, pp. 2554-2563, 2014.
[43] Y. Li, S. Xiao, M. Rotaru, J.K. Sykulski, A dual kriging approach with improved points selection algorithm for memory efficient surrogate optimization in electromagnetics, art no. 7000504, IEEE Trans. Magn. 52 (3) (2016) 1–4. art no. 7000504.
[44] P. Barmuta, F. Ferranti, G.P. Gibiino, A. Lewandowski, D.M.M.P. Schreurs, Compact behavioral models of nonlinear active devices using response surface methodology, IEEE Trans. Microw. Theory Tech. 63 (1) (2015) 56–64.
[45] F. Feng, W. Na, W. Liu, S. Yan, L. Zhu, J. Ma, Q.J. Zhang, Multifeature-assisted neuro-transfer function surrogate-based EM optimization exploiting trust-region algorithms for microwave filter design, IEEE Trans. Microw. Theory Techn. 68 (2) (2020) 531–542.
[46] J. Cai, C. Yu, L. Sun, S. Chen, J.B. King, Dynamic behavioral modeling of RF power amplifier based on time-delay support vector regression, IEEE Trans. Microw. Theory Techn. 67 (2) (2019) 533–543.
[47] A. Petrocchi, A. Kaintura, G. Avolio, D. Spina, T. Dhaene, A. Raffo, D.M.P.-P. Schreurs, Measurement uncertainty propagation in transistor model parameters via polynomial chaos expansion, IEEE Microw. Wirel. Comp. Lett. 27 (6) (2017) 572–574.
[48] Z. Zhou, Z. Wei, J. Ren, Y.X. Sun, Y. Yin, G.F. Pedersen, M. Shen, Bayesian-inspired sampling for efficient machine-learning-assisted microwave component design, IEEE Trans. Microw. Theory Techn. 72 (2) (2024) 996–1007.
[49] J. Ma, J. Qiao, G. Watkins, S. Dang, R. Piechocki, J. Haine, M. Beach, Revolutionizing microwave circuit design with machine learning: challenges and opportunities, IEEE Comm. Mag. 62 (8) (2024) 100–106.
[50] S. Koziel, A. Pietrenko-Dabrowska, Optimization of microwave components using machine learning and rapid sensitivity analysis, paper no. 31265, Sc. Rep. 14 (2024). paper no. 31265.
[51] F. Garbuglia, D. Spina, D. Deschrijver, I. Couckuyt, T. Dhaene, Bayesian optimization for microwave devices using deep GP spectral surrogate models, IEEE Trans. Microw. Theory Techn. 71 (6) (2023) 2311–2318.
[52] A. Toktas, D. Ustun, M. Tekbas, Multi-objective design of multi-layer radar absorber using surrogate-based optimization, IEEE Trans. Microw. Theory Techn. 67 (8) (2019) 3318–3329.
[53] B.S. Chouhan, A. Nawaz, A. Das, K.M. Rohith, A. Ahmad, G. Kumar, Machine learning-driven ultra-broadband terahertz multilayer metamaterial, J. Light. Techn. 43 (6) (2025) 2734–2744.
[54] N. Taran, D.M. Ionel, D.G. Dorrell, Two-level surrogate-assisted differential evolution multi-objective optimization of electric machines using 3-D FEA, paper ID 8107605, IEEE Trans. Magn. 54 (11) (2018). paper ID 8107605.
[55] J.W. Bandler, Q.S. Cheng, S.A. Dakroury, A.S. Mohamed, M.H. Bakr, K. Madsen, J. Sondergaard, Space mapping: the state of the art, IEEE Trans. Microw. Theory Tech. 52 (1) (2004) 337–361.
[56] S. Li, X. Fan, P.D. Laforge, Q.S. Cheng, Surrogate model-based space mapping in postfabrication bandpass filters' tuning, IEEE Trans. Microw. Theory Tech. 68 (6) (2020) 2172–2182.
[57] S. Koziel, S.D. Unnsteinsson, Expedited design closure of antennas by means of trust-region-based adaptive response scaling, IEEE Antennas Wirel. Prop. Lett. 17 (6) (2018) 1099–1103.
[58] S. Koziel, Shape-preserving response prediction for microwave design optimization, IEEE Trans. Microw. Theory Tech. 58 (11) (2010) 2829–2837.
[59] C. Zhang, F. Feng, V. Gongal-Reddy, Q.J. Zhang, J.W. Bandler, Cognition-driven formulation of space mapping for equal-ripple optimization of microwave filters, *IEEE Trans*, Microw. Theory Techn 63 (7) (2015) 2154–2165.

[60] A. Pietrenko-Dabrowska, S. Koziel, Response feature technology for high-frequency electronics. Optimization, modeling, and design automation, Springer, New York, 2023.
[61] M. Xi, et al., A machine-learning-assisted antenna array isolation optimization method using intelligent surfaces for bistatic in-band full-duplex communication systems, IEEE Trans. Ant. Propag. 73 (2) (2025) 962–974.
[62] S. Koziel, M. Abdullah, S. Szczepanski, Design of high-performance scattering metasurfaces through optimization-based explicit RCS reduction, IEEE Access. 9 (2021) 113077–113088.
[63] X. Han, H. Xu, Y. Chang, M. Lin, Z. Wanyuan, X. Wu, X. Wei, Multiple diffuse coding metasurface of independent polarization for RCS reduction, IEEE Access. 8 (2020) 162313–162321.
[64] S. Chen, M. Guo, K. Xu, P. Zhao, L. Dong, G. Wang, A frequency synthesizer based microwave permittivity sensor using CMRC structure, IEEE Access. 6 (2018) 8556–8563.
[65] S. Koziel, Improved trust-region gradient-search algorithm for accelerated optimization of wideband antenna input characteristics, Int. J. RF & Microw. CAE 29 (4) (2019) e21567.
[66] A. Pietrenko-Dabrowska, S. Koziel, Expedited antenna optimization with numerical derivatives and gradient change tracking, Eng. Comp. 37 (4) (2019) 1179–1193.
[67] A. Pietrenko-Dabrowska, S. Koziel, Rapid antenna optimization with restricted sensitivity updates by dominant direction identification, Knowl. Based Syst. 268 (paper 110453) (2023).
[68] J. Li, A. Yang, C. Tian, L. Ye, B. Chen, Multi-fidelity Bayesian algorithm for antenna optimization, J. Syst. Eng. Electr. 33 (6) (2022) 1119–1126.
[69] S. Koziel, A. Pietrenko-Dabrowska, Globalized parameter tuning of microwave passives by dimensionality-reduced surrogates and multi-fidelity simulations, Sc. Rep. 15 (paper 21776) (2025).
[70] S. Koziel, Computationally efficient multi-fidelity multi-grid design optimization of microwave structures, Appl. Comp. Electromagn. Soc. J. 25 (7) (2010) 578–586.
[71] L. Leifsson, S. Koziel, Simulation-driven aerodynamic design using variable-fidelity models, Imperial College Press, London, 2015.
[72] S. Koziel, A. Pietrenko-Dabrowska, P. Plotka, Reduced-cost microwave design closure by multi-resolution EM simulations and knowledge-based model management, IEEE Access. 9 (2021) 116326–116337.
[73] S. Koziel, X.S. Yang, Q.J. Zhang (Eds.), Simulation-driven design optimization and modeling for microwave engineering, Imperial College Press, London, 2013.
[74] A.R. Conn, N.I.M. Gould, and P.L. Toint, *Trust Region Methods*, MPS-SIAM Series on Optimization, 2000.
[75] CST Microwave Studio, Dassault Systemes, France, 2025.
[76] S. Koziel, A. Pietrenko-Dabrowska, Reduced-cost electromagnetic-driven optimization of antenna structures by means of trust-region gradient-search with sparse Jacobian updates, IET Microw. Ant. Prop. 13 (10) (2019) 1646–1652.
[77] W. Na, T. Bai, D. Jin, H. Xie, W. Zhang, Q.-J. Zhang, Advanced neural space mapping-based inverse modeling method for microwave filter design, IEEE Microw. Wirel. Techn. Lett. 35 (1) (2025) 12–15.
[78] J.E. Rayas-Sánchez, et al., Microwave modeling and design optimization: the legacy of John Bandler, IEEE Trans. Microw. Theory Techn. 73 (1) (2025) 87–101.
[79] A. Pietrenko-Dabrowska, S. Koziel, Surrogate modeling of impedance matching transformers by means of variable-fidelity EM simulations and nested co-kriging, Int. J. RF Microw. CAE 30 (8) (2020) e22268.
[80] S. Koziel, A. Pietrenko-Dabrowska, Expedited optimization of antenna input characteristics with adaptive Broyden updates, Eng. Comp. 37 (3) (2019).
[81] Z. Lin, Q.-X. Chu, A novel approach to the design of dual-band power divider with variable power dividing ratio based on coupled-lines, Prog. Electromagn. Res. 103 (2010) 271–284.
[82] S. Koziel, A. Pietrenko-Dabrowska, Reliable data-driven modeling of high-frequency structures by means of nested kriging with enhanced design of experiments, Eng. Comp. 36 (7) (2019) 2293–2308.
[83] D.A. Letavin, S.N. Shabunin, Miniaturization of a branch-line coupler using microstrip cells, Int. Sci. Tech. Conf. Actual. Probl. Electron. Instrum. Eng. (APEIE) (2018) 62–65.